Morphological Partitioning of Ethylene Defects in Random Propylene−Ethylene Copolymers†

Rufina G. Alamo*

Department of Chemical Engineering, Florida Agricultural and Mechanical University−Florida State University, 2525 Pottsdamer Street, Tallahassee, Florida 32310-6046

D. L. VanderHart*

Polymers Division, National Institute of Standards and Technology, Gaithersburg, Maryland 20899-8544

Marc R. Nyden

Building and Fire Research Laboratory, National Institute of Standards and Technology, Gaithersburg, Maryland 20899-8544

L. Mandelkern

Department of Chemistry, Florida State University, Tallahassee, Florida 32306

Received February 14, 2000; Revised Manuscript Received May 11, 2000

ABSTRACT: A series of four propylene/ethylene, metallocene-catalyzed random copolymer samples, with ethylene mole fractions ranging from 0.8% to 7.5% and melt crystallization histories of cooling at 1 °C/min, were studied by ^{13}C solid-state NMR techniques. The principal objective of the study was to determine the partitioning of the ethylene "defect" residues within the semicrystalline morphology of these isotactic poly(propylene/ethylene) copolymers. Signals from the crystalline (CR) and the noncrystalline (NC) regions were separated on the basis of contrasting $T_{1\rho}^{H}$ behaviors. Four new resonances, three distinct and one strongly overlapping, were identified in the spectrum of the CR regions. The assignment of these new defect resonances to specific carbons at or near the ethylene defect site was made principally on the basis of quantum mechanical chemical shift calculations. These calculations were performed on two methyl-terminated oligomers of about 6.5 monomers in length with a 3_1 helical backbone conformation, characteristic of the iPP backbone conformation in the CR state. One oligomer was the pure iPP chain, and the other contained one centrally located ethylene repeat unit. Good agreement between the experimental shifts associated with the ethylene defect and the computed shifts supported the assumption that the chain conformation in the CR regions in the vicinity of the ethylene defect remained a 3_1 helix. This good agreement between shifts was obtained when the computed shifts were not used directly, but used in a difference mode. This mode was based on the computed shift differences for corresponding carbons on the two oligomers where these differences were applied to the experimental shifts of the main iPP peaks with the same chemical identity. The assignment of the defect resonances, along with the loss of chemical shift equivalences seen in solution-state spectra, was also rationalized in the context of γ-gauche and vicinal−gauche interactions as applied to the 3_1 helical structure. Defect line width differences that parallel the line width differences of the main iPP resonances also aid in assigning the defect resonances to particular types of carbons. Over the range of ethylene concentrations studied herein, the partitioning coefficient, P_{CR}(eth), given by the ratio of the *concentration* of ethylene residues in the CR region to the sample-average *concentration* of ethylene residues, is found to be constant, taking a value of 0.42 with a standard uncertainty of 0.03. On the basis of measurements of the NMR crystallinities, this partitioning translates to a fraction of the total ethylene residues in CR regions ranging from 0.24 to 0.30 and an average concentration of ethylenes in the NC region about twice the overall concentration. We also looked for evidence that the ethylene residues become highly concentrated at the CR/NC interface. While we cannot say whether this is happening on the NC side of the interface, since we cannot identify any NC defect resonances, we can claim that a high concentration of ethylene residues is *not* found on the CR side near the interface.

Introduction

It is a matter of technical and scientific interest that small fractions of α-olefin comonomers, randomly incorporated into isotactic polypropylene (iPP) chains, can significantly influence material properties. Impact strength and hardness can be varied continuously with increasing comonomer content. Materials based on these commodity polyolefins can, thus, be tailored for specific applications. Reports, although not as numerous as for ethylene−1-alkene copolymers, on thermal,[1,2] structural,[3−5] morphological,[6,7] and polymorphic[6,8,9] properties of propylene−ethylene copolymers with very minor ethylene contents have been published including some on crystallization kinetics.[2,6,7,10,11] Issues of fundamental relevance in the analysis of some of these properties, such as the cocrystallizability of the ethylene and propylene units, are generally treated "indirectly" from the analysis of thermal or X-ray scattering data.[3−5] We

† Paper presented at the Symposium on Semicrystalline Polymers in Memory of Andrew Keller, ACS Meeting, New Orleans, Aug 22−26, 1999. Divison of Polymeric Materials: Science and Engineering.

* To whom correspondence should be addressed.

10.1021/ma000267i CCC: $19.00
Published on Web 07/21/2000

Table 1. Molecular Characterization of Propylene−Ethylene Random Copolymers[a]

copolymer	M_w (g/mol) (±10% of the value)	M_w/M_n (±0.3)	2,1 erythro[b,c]/ 1000 (±0.2)	2,1 erythro[b,d]/ 1000 (±0.2)	stereo/1000[b] (mainly *mrrm*)	comonomer[b,e]/ 1000	total defects[b]/ 1000	T_m (°C)[f] (±0.5)
iPP/0.8 Eth	233 100	2.0	1.8	2.1	5.7(3)	7.9(5)	17.3(12)	134.0, 143.4
iPP/2.2 Eth	214 800	1.8	4.7	0.0	7.0(3)	22.0(7)	33.7(12)	127.0, 137.0
iPP/4.6 Eth	251 000	2.1	3.2	1.0	8.1(4)	45.9(5)	58.2(13)	121.6
iPP/7.5 Eth	188 000	1.7	3.6	0.0	8.2(4)	74.7(10)	86.5(16)	108.0

[a] Standard uncertainties either appear in the column heading or are given in parentheses in units of the last significant figure. Molar concentrations are defined per 1000 repeat units. [b] Molar concentrations. [c] Bonded to an ethylene group. [d] Isolated 2,1 erythro. [e] From isolated comonomer. The total ethylene content is calculated by adding to the data of this column the fractional contents in column 4. [f] Measured by DSC. Data taken as the peak of the endotherm/s.

are not aware of any previous direct NMR determinations that have dealt with how the comonomer unit is partitioned among the different phases in these solid polymers. Similar issues in random copolymers of ethylene with α-olefins are better known. Linear low-density polyethylene (LLDPE) of the heterogeneous and homogeneous type as well as model random ethylene copolymers have been studied, and in general, consensus has been reached about the cocrystallizability of the branches or structural irregularities and the ethylene backbone units. By direct and indirect techniques of analysis, it is concluded that a small percentage of small branches such as methyl, chlorine, and others are included in the crystalline lattice; larger branches are mainly excluded.[12]

In the reported studies of random propylene copolymers, unfractionated Ziegler−Natta-type of samples or fractions from a Ziegler−Natta whole polymer[2,4,6,9] were studied. These types of polypropylenes have a broad distribution of molecular mass and a heterogeneous distribution of comonomer composition from chain to chain. While careful fractionation yields a more homogeneous product relative to both distributions, still some heterogeneities remain.[13] The fact that ethylene is a smaller monomer than propylene might lead one to expect that the ethylene comonomer would easily fit into the iPP lattice. Alternatively, the substitution of a proton for a methyl group in the iPP lattice creates a small hole which will diminish, to some extent, the van der Waals energy of that lattice. It is, thus, not surprising to find contradictory conclusions as to whether the ethylene is or is not included in the polypropylene crystalline lattice. The observed high levels of crystallinity,[4] invariance of crystallite thickness with increasing comonomer content,[5] and molecular mechanics calculations on model compounds[14] led to the proposal that the ethylene units were partially included in the crystal. In other reports, the decrease of the melting temperature with increasing comonomer concentration,[2,7,15] and the invariance of both the heat of fusion, (normalized to the degree of crystallinity) and the electron density difference between crystalline and amorphous phases with increasing ethylene content,[3] led these authors to conclude that the ethylene units are rejected from the crystal.

In the present study the inclusion of the ethylene units in the crystal is investigated by isolating the ^{13}C NMR line shape associated with the crystalline (CR) phase and then assessing the relative intensities of those ethylene-related resonances belonging to the CR phase. To avoid the complexities that are associated with the analysis of properties of compositionally heterogeneous Ziegler−Natta-type polypropylenes, all of the polypropylenes studied were synthesized with the same metallocene-type catalyst. In these samples the ethylene composition distribution from chain to chain is narrow, and the intramolecular sequence distribution is random. Thus, these materials differ from the propylene−ethylenes studied previously in that the measured average ethylene content is more representative of the content of any constituent molecule instead of being an average over separate populations of chains, each having different average ethylene content.[16]

The distribution of the ethylene units among the different phases in the solid polymer can be analyzed by comparing the concentration of ethylene in the crystal with respect to the sample-wide ethylene concentration. Thus, following the nomenclature introduced in a previous paper,[17] the crystalline partitioning coefficient, $P_{CR}(\text{eth})$, for the ethylene units is defined as the ratio between these two values:

$$P_{CR}(\text{eth}) = C_{CR}(\text{eth})/C_{Ave}(\text{eth})$$

where $C_{CR}(\text{eth})$ is the concentration of ethylene in the crystalline region and $C_{Ave}(\text{eth})$ is the average concentration of ethylene in the sample, determined by solution-state NMR. The partitioning coefficient indicates the level of acceptance of the ethylene "defect" by the process of crystallization; $P_{CR}(\text{eth}) = 1$ means there is full acceptance while $P_{CR}(\text{eth}) = 0$ signifies full rejection.

In the present work, we will determine $P_{CR}(\text{eth})$ for a series of propylene−ethylenes with increasing ethylene content. Such a determination requires both that we identify those new resonances which are associated with the ethylene monomer and that we assign correctly the number of carbons per defect contributing to each new resonance. Central to this latter assignment activity is the comparison of the experimental ^{13}C NMR resonances with calculated NMR chemical shifts from quantum mechanical calculations. The theoretical methods are based on density functional theory[18] and were carried out for a single, methyl-terminated iPP whose backbone conformation was assumed to be a 3_1 helix, characteristic of all iPP crystal lattices.

Experimental Section

Uncertainties in experimentally determined quantities appearing in this paper and expressed in the form "$a \pm b$" will be understood to mean that "b" is a *standard uncertainty*.

The molecular characterization of the propylene−ethylene copolymers studied is given in Table 1. These copolymers are experimental samples obtained with the same metallocene-type catalyst.[19] Thus, the molecular mass and concentration of stereo- and regio-type defects are very similar for all of them. Besides the structural irregularity introduced in the chain by the comonomer, the samples have a similar mole fraction of defects introduced by tacticity (0.70 ± 0.13)% and very similar mole fractions of misinsertions of the 2,1 erythro type (0.42 ± 0.07)%. The 1,3 defect, which effectively inserts a *n*-propyl group into the backbone sequence, was absent in these

samples. Four copolymers with ethylene mole fractions varying from 0.8 to 7.5% were studied. We will use the designation, iPP/"*X*" Eth, for these copolymers where "*X*" is the numerical value of the mole fraction of ethylene, expressed in percent (e.g., iPP/0.8 Eth). Also listed in this table are the mole fractions, or concentrations, of all types of defects and the melting temperatures.

The molecular masses and their distributions were determined by standard gel permeation chromatography methods.[20] Calibration was carried out with polystyrene standards. The type and fractional content of all the defects were obtained from 75 MHz solution-state ^{13}C NMR spectra taken with random noise, proton decoupling. The NMR spectrometer was manufactured by Bruker Instruments. Approximately 5000 scans were added using an acquisition time of 1.36 s and a recycle delay of 20 s with nuclear Overhauser enhancement. Spectra were obtained at 125 °C in deuterated tetrachloroethane using 10 mm o.d. sample tubes and solutions with about 0.15 mass fraction of polymer. The assignment of resonances to defects was based on published assignments.[21] Two of the copolymers show four different defects that disrupt the isotactic sequence, namely:

(a) a misinsertion (2,1 erythro defect) followed by an ethylene addition

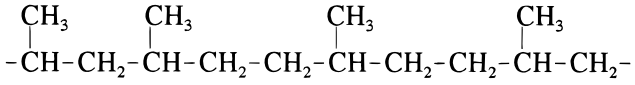

(b) an isolated 2,1 erythro misinsertion (subsequently corrected)

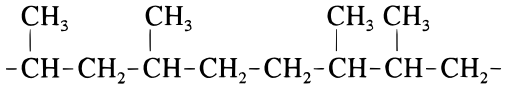

(c) an isolated ethylene insertion

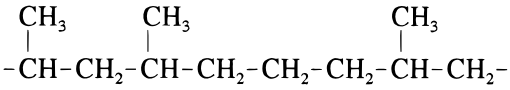

(d) stereo defects mainly represented by the sequence $-mmmrrmmm-$

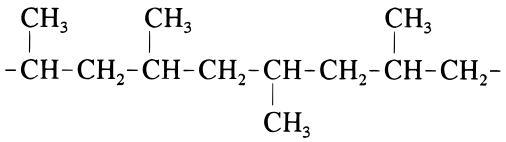

The ^{13}C NMR spectra of iPP/2.2 Eth and of iPP/7.5 Eth did not show resonances in the region of the isolated 2,1 erythro misinsertions (42.5 ppm).

The copolymers were crystallized from the melt (190 °C) at a cooling rate of 1 °C/min following the same experimental conditions detailed in a previous work.[17] For the solid-state ^{13}C NMR experiments, cylinders (6 mm o.d. and 12 mm high) were machined from larger rods to fit into a 7 mm o.d. rotor. All spectra were taken at ambient temperature at 2.35 T (25.2 MHz) using a noncommercial spectrometer with a noncommercial probe that incorporated a magic-angle-spinning (MAS) rotor/stator manufactured by Doty Scientific, Inc.[22] The MAS frequency was 4.0 kHz, and the ^{13}C and ^{1}H radio-frequency field strengths, as they pertain to both cross-polarization (CP) and proton decoupling, corresponded to nutation frequencies of 66 and 62 kHz, respectively. The recycle period between acquisitions was 5 s, and the acquisition time, under high-power decoupling, was 140 ms. The fundamentals of the NMR method used to isolate the spectra of the noncrystalline (NC) and crystalline (CR) components have been detailed in previous works.[17,23] These "CR" and "NC" spectra are generated using linear combinations of two experimental CPMAS spectra. Conditions for acquiring these latter two spectra have in common a 0.7 ms CP time which immediately follows differing proton spin-locking (SL) periods (0 ms and a second time in the 6−8 ms range). Rotating-frame proton relaxation, $T_{1\rho}^{H}$, a dissipative process sensitive to motions in the mid-kilohertz range, is active during spin-locking. Since $T_{1\rho}^{H}(NC) \ll T_{1\rho}^{H}(CR)$ in iPP under these conditions, a 0 ms SL spectrum will have a stronger relative contribution from the NC region than will, say, a 7 ms SL spectrum of the same sample. Hence, corresponding "CR" spectra would be more strongly weighted by the 7 ms SL spectrum (there being a minor portion of the 0 ms SL spectrum subtracted in order to null the NC contributions) while the "NC" spectrum would be strongly weighted toward the 0 ms SL spectrum.

The fact that "spin diffusion"[24] is present in the SL period is both good and bad. It is good in that the proton polarization, locally, remains uniform, regardless of very local variations in mobility. (Thus, one is assured that during SL protons on defects behave very similarly to their nondefect proton neighbors. In this way, carbons on defects inside the CR regions will be included as CR carbons, even if the mobility near such a defect differs from the usual mobility within the CR region.) It is bad in that there is some blurring of the true distinctions between carbons in CR versus NC environments. For example, a spin diffusion modeling[17] of this $T_{1\rho}^{H}$-based method for separating the CR and NC spectral contributions shows that, on a per-carbon basis in the CR spectrum, carbons in the interior of a given crystallite contribute more strongly than do those near the CR/NC interface. Moreover, even NC carbons very close to the interface give a positive, weak contribution, this latter contribution being offset by a negative contribution from carbons in the interior of the NC region. Owing to the weakness of the defect resonances, between 30 000 and 70 000 scans were collected for each sample to increase the signal-to-noise ratio of the spectra.

Melting temperatures and heat of fusion of the same samples were obtained in a differential scanning calorimeter (Perkin-Elmer DSC-7) using ≈4 mg of sample and a heating rate of 10 °C/min. Static temperature calibration of the instrument was carried out with indium.

Results and Discussion

Generation and Analysis of Spectra. An illustration of the method used to isolate the spectrum of the crystalline ("CR") region is shown in Figure 1. Here the spectrum generated with zero spin-locking time (Figure 1A) corresponds more closely to equal weighting from all components. This spectrum shows more intense, broader wings from the contribution of the noncrystalline ("NC") regions than the spectrum generated with 6 ms spin-locking (SL) time, prior to cross-polarization (Figure 1B); this latter spectrum has stronger relative contributions from those carbons in the CR regions. The 6 ms SL spectrum has been multiplied by 1.4 to match peak intensities with those of the 0 ms SL spectrum in order to match the magnitudes of the CR region. To isolate the spectrum of the CR region, the smaller fractional NC content of the 6 ms SL spectrum is eliminated by subtraction of a properly scaled 0 ms SL spectrum. This scaling factor is chosen to be the largest number satisfying the criterion that the difference spectrum contains no regions with negative intensity in the spectral region between 10 and 60 ppm. This latter criterion makes use of the fact that the NC carbons have the broader resonances; hence, there are spectral regions where only the NC carbons contribute. The line shape of the resulting CR spectrum (Figure 1C) is characterized by much sharper spectral features as seen in the figure. Similarly, the NC line shape (Figure 1D) is obtained by subtracting some of the 6 ms SL spectrum (the CR contribution) from the 0 ms SL

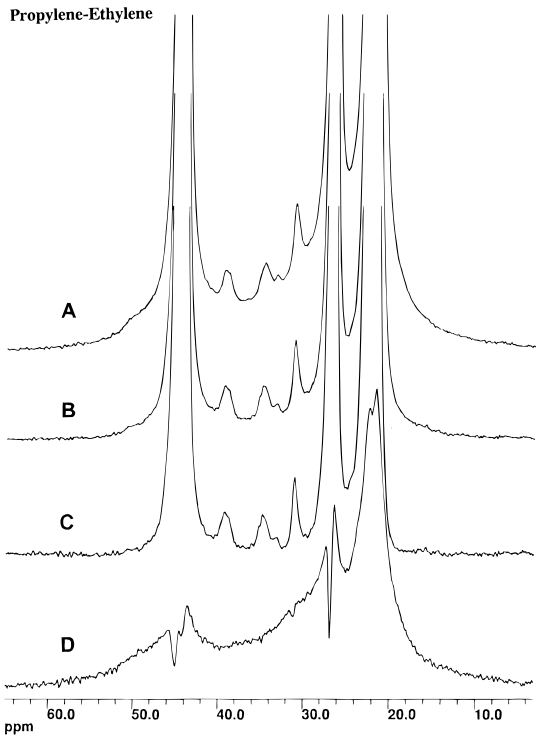

Figure 1. Illustration of the method of extracting line shapes of the crystalline (CR) and noncrystalline (NC) regions for sample iPP/7.5 Eth: experimental 0 ms spin-lock (SL) spectrum (A); experimental 6 ms SL spectrum multiplied by 1.4 in order to equalize the CR contributions with the top spectrum (B); deduced CR spectrum (C); deduced NC spectrum (D). The lower two spectra are linear combinations of the upper two spectra; also, the sum of the CR and the NC spectrum is the top spectrum.

spectrum. The method used and the nonideal morphology of these iPP's both contribute some approximate character to these line shapes. While a more detailed description and interpretation of the CR and NC line shapes appears in our preceding publication,[17] we will highlight two qualitative points. First, owing to the presence of spin diffusion, an iPP sample with an idealized two-phase morphology (with spatially sharp interfaces) would yield CR and NC line shapes with the following features: These line shapes would more heavily weight the contributions of carbons in the interior of the desired region and less heavily those carbons near the interface of the desired region. In addition, there would be smaller positive contributions from carbons in the undesired region near the interface and these contributions would be offset by negative contributions from carbons in the interior of the undesired regions. Thus, for example, the NC line shape would only give a good null of the CR contributions if the line shape for each chemically distinct carbon were *not* a function of distance from the interface. However, in Figure 1, one cannot, in attempting to generate the NC spectrum, obtain a good null of the CR resonances. Therefore, this leads to the second point, namely, that it is certainly an approximation to say that an iPP sample is an ideal, two-phase system. The transition from a high degree of order in the CR region to the disorder of the NC region takes place over a finite distance. In the NC spectrum of Figure 1, the combination of sharper negative-going features with slightly broader, positive-going features is proof that carbons in the interior of the CR phase have slightly narrower resonances than do those corresponding CR carbons closer to the interface.

In evaluating this method of separating CR and NC signals, precision is sacrificed when one recognizes the nonuniform sampling across regions and the contamination of the signals from the regions one wishes to eliminate. However, it is to our advantage that there are positive contributions to both the CR and the NC line shapes from *both* sides of the interface. The latter feature allows us to address the question whether defects are highly concentrated at the interface; if they are, the defect resonances will contribute in a nontrivial way both to the CR and the NC line shapes. We will presently use the fact that the defect resonances are absent from the NC spectrum in Figure 1 to argue that the defects are not highly concentrated on the CR side of the interface. Meanwhile, it is against this backdrop that we will treat the defect resonances that are seen in the CR spectra as though they arose from a uniform distribution throughout the CR region.

Sharp well-defined resonances are observed in the "CR" spectrum of Figure 1. These include the backbone carbon resonances corresponding to the methyl carbons (22.1 ppm), the methine carbons (26.7 ppm), and the methylene carbons (44.5 ppm). In addition to the backbone resonances, three well-defined sharp resonances, which we will presently show to be associated with the comonomer, are observed at 31.2, 34.7, and 39.3 ppm. A weaker resonance at 33.3 ppm is associated with the stereo defects, as will be discussed later. The resonances of the NC spectrum are broader than those of the CR for two reasons: (a) motions, even anisotropic motions, with significant spectral densities in the mid-kilohertz range, cause broadening,[25] and (b) there are dispersions of chemical shifts associated with the different, motionally averaged microenvironments found in a disordered material. The absence of any distinct defect resonances in the NC spectrum of Figure 1 underscores the fact that *defects in disordered iPP regions at ambient temperature have associated carbon resonances which are too broad and weak to be identified against the broad NC iPP resonances.* An important corollary is that *all defect resonances that we are able to distinguish arise from ordered, not disordered, regions.* This means, for example, that, relative to the question of whether defects concentrate at the interface, we can only comment on the possibility that they concentrate on the CR side of the interface; we will be unable to comment on whether they concentrate on the NC (disordered) side of the interface.

The full "CR" spectra of the four different propylene−ethylene copolymers studied are displayed with increasing ethylene content in Figure 2. These spectra are all normalized to the same total intensity. There is a slight deterioration of resolution as the ethylene content increases; this is most notable for the methylene resonance at 44 ppm. We also know that the crystallites in these samples show polymorphy;[26] both the γ-form[27,28] and the α-form[29−31] are present. The mass fraction of the total CR fraction that is γ-phase was estimated from DSC heats of fusion for each copolymer.[26] In order of increasing ethylene content, values of 0.45, 0.40, 0.70, and 1.00 were obtained. Thus, in general, the content of the γ-allomorph formed in the copolymer increased with increasing concentration of comonomer. This trend has also been observed in homopolymers with increasing concentrations of stereo or regio defects.[26] It was also

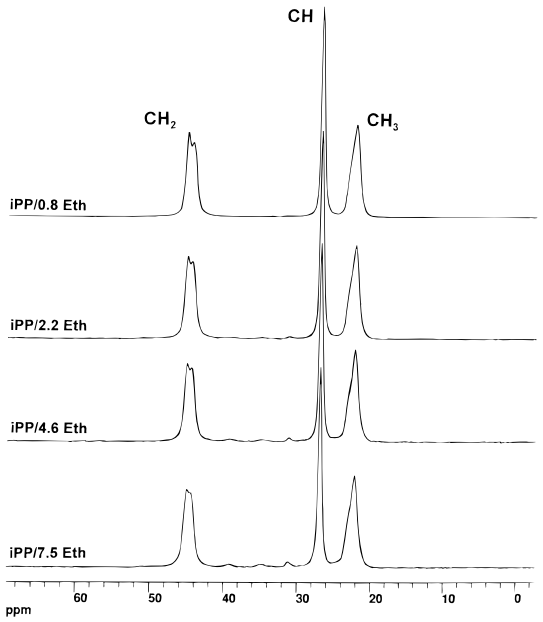

Figure 2. The 25.2 MHz ^{13}C CPMAS CR spectra of the four samples studied. Spectra are normalized to the same total intensity.

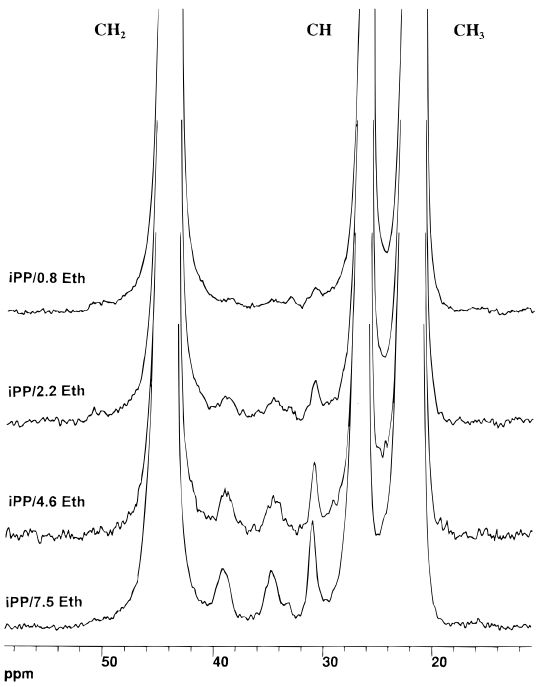

Figure 3. Vertically amplified CR spectra of Figure 2.

observed[26] that the formation of the γ-polymorph is favored with increasing crystallization temperature. The relatively slow crystallization of the propylene−ethylene copolymers in the present study leads to relatively high contents of the γ-polymorph.

On the basis of literature reports, line shape changes, especially in the methyl region, are also expected to accompany conversion of the α allomorph to the γ-allomorph.[32,33] Given that the isolated-chain conformation for both the α- and γ-allomorphs is a 3_1 helix,[27−31] those carbons closer to the perimeter of the helix, namely, the methyl and methylene carbons, are most sensitive to changes in the crystal packing. The methine carbon, in contrast, is quite sheltered within the helix and displays a corresponding sharper resonance. Each allomorph exhibits methyl and methylene resonances with multiple components owing, at least in part, to the fact that some of the symmetry operations of the 3_1 helix are not the symmetry operations of the lattice. In Figure 2, the line shape changes that occur as a function of ethylene content are quite subtle, and we will not argue that the NMR line shape clearly supports the increasing dominance of the γ-allomorph as the ethylene concentration increases. Our reluctance to make this connection also stems the significant line shape changes which occur upon annealing.[34] In our own experience, significant line shape changes can be as much related to thermal history as to the α/γ ratio.

Figure 3 shows the normalized spectra of Figure 2 vertically magnified. One can see that the three resonances associated with the ethylene defect increase with the overall ethylene concentration. In Figure 4 we illustrate that, within the signal-to-noise ratio, the concentration of ethylene defects in the CR region for the copolymers with ethylene mole fractions of 4.6% and 7.5% is proportional to the overall ethylene concentration. In Figure 4A,B, total integrals are proportional to the inverse of the overall ethylene concentrations. The fact that the defect resonances are nulled in the difference spectrum supports the foregoing conclusion.

Identification and Assignment of Distinguishable Ethylene-Defect Resonances. It is expected that

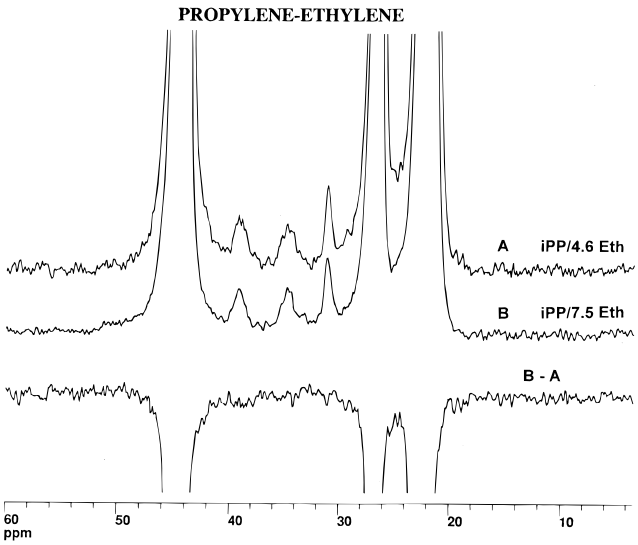

Figure 4. Spectra illustrating that, for the iPP/4.6 Eth and the iPP/7.5 Eth samples, the intensity of the defect resonances is proportional to the overall concentration of the defects: (A) CR spectrum of iPP/4.6 Eth with total intensity = 7.5/4.6; (B) CR spectrum of iPP/7.5 Eth with total intensity of 1.00. Lower spectrum = (B) − (A). Lack of defect-resonance intensity in this difference spectrum illustrates this point.

the relative intensity of resonances corresponding to the ethylene in the crystalline region will increase with the overall average ethylene content. In Figure 3, the three resonances, cited earlier as being associated with the ethylene defect, show this behavior; hence, they are indeed associated with the ethylene defect. However, other resonances, in addition to those specific to the ethylene group, are also present in these spectra, and their relative intensity is most obvious in the iPP/0.8 Eth CR spectrum. In a previous work, resonances in the CR spectrum associated with the stereo-*mrrm* and regio-2,1 erythro defects have been found at (16.0, 30.1, 33.1, 47.9, 50.6) ppm for that stereo defect and at (11.5, 31.6, 33.1, 35.3) ppm for that regio defect. Thus, the additional resonances are the contributions to the iPP/0.8

Eth CR spectrum from the stereo and regio structural irregularities. Both the 31.1 and 34.7 ppm resonances of the ethylene defect overlap with resonances from the stereo and regio defects. Fortunately, the resonance at 39.2 ppm is free of overlaps with resonances from these defects and, thus, can be used to quantify unambiguously the ethylene concentration in the crystal provided that the type of carbon and number of carbons that contribute to this resonance are first identified.

In the CR iPP/7.5 Eth spectrum of Figure 3, the ethylene defect resonances are very dominant among the defect resonances. Integration of each of these peaks leads to the conclusion that the integrals of these peaks are very close to being in a 1:1:1 ratio. The second piece of information about these defect resonances is surmised and is based on line width analogies. Given that we might expect the 3_1 helical character of the CR chain to be preserved in the vicinity of the ethylene defect (the ethylene monomer is smaller than the propylene monomer and would produce no strong steric barrier against the formation of this helix), we would presume that the 31.1 ppm line is a methine resonance (the resonance is relatively narrow, as is the main CR methine resonance) and that the 34.7 and 39.2 ppm resonances are both methylene resonances. (Both line widths are very similar to the main methylene and methyl line widths; however, the more downfield chemical shift tends to eliminate the possibility that either of these lines belongs to a methyl carbon.)

An unambiguous assignment of the defect resonances to particular carbons is necessary in order to be confident about the deduced CR partitioning coefficient for ethylene groups in iPP. We might be tempted to use solution-state chemical shifts to help in this assignment, even though we are aware that the frozen conformation of the iPP chain in the CR regions, compared to the dynamic averaging over multiple conformations in the solution state, will likely create disparities between the solution-state shifts and the solid-state shifts. If we consider the isolated ethylene defect, [...−$CH(CH_3)$−CH_2−$CH(CH_3)$−CH_2−C*H_2−CH_2−$CH(CH_3)$−CH_2−$CH(CH_3)$−...], there is a symmetry of structure about the central methylene carbon in the sequence of three methylenes created by the ethylene repeat unit. The solution state shifts reflect that symmetry; therefore, all distinct resonances associated with the ethylene defect represent two carbons per defect, except the resonance of the central carbon that represents a single carbon. Starting with the central carbon and moving outward along the backbone, solution state shifts are[21] respectively 24.1, 37.8, 30.8, and 46.1 ppm. If these solution-state shifts coincide with the solid-state shifts, then the central-carbon resonance should be obscured by the main CH and CH_3 peaks, and the 31.1 ppm peak would be a CH resonance, as presumed from line width considerations. The problem is that the 37.8 and 46.1 ppm CH_2 values only partially match with the observed solid-state values of 34.7 and 39.2 ppm. Hence, from these grounds we doubted whether each solid-state defect resonance represents two carbons per defect.

Given our expectation that the 3_1 helical conformation will be preserved in the vicinity of the ethylene defect, we can argue that chemically similar carbons on opposite sides of the central CH_2 carbon (see foregoing paragraph) are inequivalent. To do this, we invoke some solid-state, alkane, chemical-shift correlations with conformation, namely, the γ-gauche effect (showing an upfield shift of about 5 ppm per γ-gauche interaction[35]) and the vicinal−gauche effect (showing an upfield shift of about 2.5 ppm per vicinal−gauche interaction[36]). For any backbone carbon in a 3_1 helix there are inequivalent arrangements of atoms if one looks along the chain in one direction, say the "A" direction, or in the opposite, say, the "B" direction. Consider, for example, the γ-gauche effect. This effect is said to be present in an alkane for a given carbon when, three bonds away from that carbon, there is another carbon defined by a dihedral angle near ±60°. In the 3_1 helix of defect-free iPP, each CH_2 carbon sees one γ-gauche effect because there is a CH carbon in the A direction. Each CH carbon, on the other hand, sees two γ-gauche effects: one with a CH_2 carbon in the B direction and one with a CH_3 carbon in the A direction. Therefore, in creating the ethylene defect by removing a CH_3 group and substituting a H atom, one removes the γ-gauche interaction from only one of the two CH carbons that would have been "γ" to that removed methyl. Hence, one of the two nearby CH carbons should experience a downfield shift of about 5 ppm. A similar argument makes the two CH_2 carbons that are bonded to the central CH_2 carbon inequivalent. Establishing their inequivalence requires that we invoke the vicinal−gauche effect and a corresponding difference of one vicinal−gauche interaction. If a γ-gauche interaction exists between two carbons, then the two inner carbons that are involved in defining this gauche dihedral angle are each said to experience a resulting vicinal−gauche interaction. This vicinal−gauche interaction is claimed to produce an upfield shift of about 2.5 ppm, although the magnitude of this shift seems less stable[36] than in the case of the γ-gauche shift. On the basis of these arguments, one expects that the defect resonances will each represent one carbon per defect and that the three observable resonances represent the two CH_2 carbons bonded to the central carbon along with one of the adjacent CH carbons. Moreover, if the above reasoning is correct, we anticipate that the 39.2 ppm methylene carbon will lie between the central carbon and the 31.1 ppm methine carbon; also, the other adjacent CH carbon will be buried beneath the main CH peak.

Because of the importance of the assignment question, we also attempted theoretical quantum mechanical (QM) calculations of the chemical shifts for each carbon atom. As will be seen presently, the conformational arguments and assignments of the foregoing paragraph are consistent with the results of the QM calculations; however, historically these calculations were done first, and while we were aware of the significance of the γ-gauche effect in creating inequivalence, our recognition of the role of the vicinal−gauche effect came later when we tried to understand the inequivalence of the CH_2 carbons at the defect site.

Quantum mechanical calculations, in which the second derivatives of the energy with respect to the magnetic moment and magnetic field strength were evaluated for each carbon, were performed on helical oligomers of iPP, with and without a centrally located ethylene repeat unit. The coordinates corresponding to the 3_1 helical structure of crystalline iPP were obtained by modifying the coordinates reported in the work of Natta and Corradini.[37] The modifications we used were as follows: all of the C−C bond distances were set equal to 1.54×10^{-10} m, the C−C−C angles along the backbone of the chain, and the CH_3−C−C angles were

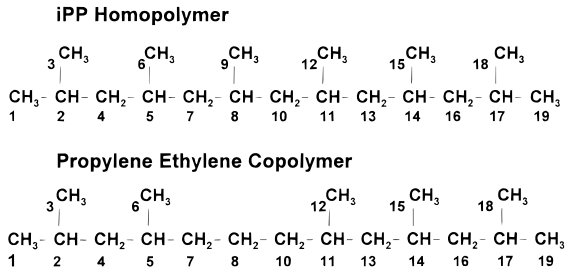

Figure 5. Oligomer of the defect-free iPP and the corresponding oligomer containing one ethylene residue. These are the oligomers, whose backbone conformations were chosen to comprise a 3_1 helix, that was used in the chemical shift calculations. Carbon numbering is included.

set at 114° and 110°, respectively, and the dihedral angles along the backbone were changed slightly so that they alternated between the values, −60° and 180°, consistent with a 3_1 helix. (The choice of +60° or −60° for the dihedral angle dictates the handedness of the helix, and we note that every proposed crystal structure for iPP incorporates both right- and left-handed helices. If one starts to build a helix of a particular handedness, it is important to choose the proper initial dihedral angle; we were careful to choose the angle that resulted in a chain with the lower energy.) The structure for the defect-containing chain was obtained by replacing one methyl group by a hydrogen in the interior of the segment (leaving the original 3_1 helix intact).

These calculations were performed at the BLYP 6-311+G(2d,p) level of theory using Gaussian 98.[38] The BLYP method, which is a pure density functional approach consisting of the Becke exchange[39] and Lee−Yang−Parr correlation functionals,[40] requires less computer time than the corresponding calculations using the hybrid B3LYP method which was recommended[18] by Cheeseman et al., who obtained reasonable agreement between experimental and computed carbon shifts for about 20 small molecules. Computation time was an important consideration because our methyl-terminated oligomers (see Figure 5) were rather large, consisting of 6.5 repeat units. We wanted to minimize end effects on the computed shifts, and to reach convergence in the computed chemical shifts, we were already straining the available resources with the computationally less demanding BLYP calculations. Although the authors of the survey[18] preferred the B3LYP calculations, their reasoning appears to be based more on its widespread use than on an appraisal of the relative accuracy of these methods for the calculation of chemical shifts. From our limited experience, accuracy appears to be comparable for these two methods.

The accuracy of these calculations can be tested by trying to reproduce the observed shifts for the defect-free iPP in a 3_1 helical conformation. If the accuracy is high, one can then perform a similar calculation on a defect-containing chain and use the results for direct comparison against the observed shifts. On the other hand, supposing that the calculations make some systematic approximations, one can take shift differences between corresponding carbons in the defect-containing and defect-free chains and use these differences as displacements from the appropriate main iPP resonances of the CR regions. In the present analysis the latter method gives better agreement with experimental results.

The calculated chemical shifts for the homopolymer and copolymer as well as the difference in chemical shifts for a given carbon number between the two types of chains are given in Table 2 where the carbon numbering is taken from Figure 5. From Table 2 we first notice that the QM calculations reproduce quite accurately the observed chemical shift for the methylenes of the homopolymer, especially the three internal ones. The calculated chemical shifts for the methyl groups excluding the ends, average 20.5 ppm. This value is also close to the observed 22.1 ppm obtained experimentally. A larger deviation is, however, found for the methines. The average calculated value (32.6 ppm) is 5.9 ppm higher than the experimental chemical shift of these type of carbons, 26.7 ppm. Thus, the accuracy of these calculations is reasonable, but it is dubious that such calculations would have sufficient significance in distinguishing between shifts of a few ppm.

Table 2. Calculated Chemical Shifts and Shift Differences for the Theoretical Oligomers of Figure 5[a]

carbon (no./type)	shift (ppm) (iPP)	shift (ppm) (comonomer)	shift diff (ppm)	predicted shift[b] (ppm)
1/CH_3	24.7	24.7	0.0	
2/CH	32.3	32.3	0.0	26.7
3/CH_3	18.8	19.0	0.2	22.3
4/CH_2	45.1	46.5	1.4	45.9
5/CH	33.4	37.8	4.4	31.1 (31.1)
6/CH_3	20.6	20.9	0.3	22.4
7/CH_2	44.2	39.4	−4.8	39.7 (39.2)
8/CH	32.3	28.1 (CH_2)	−4.2[c]	22.5 (24.5)
9/CH_3	20.4	*d*	N/A	
10/CH_2	44.1	34.9	−9.2	35.3 (34.7)
11/CH	32.3	32.4	0.1	26.8
12/CH_3	20.3	18.9	−1.4	20.7
13/CH_2	44.5	44.5	0.0	44.5
14/CH	33.0	33.0	0.0	26.7
15/CH_3	20.7	20.7	0.0	22.1
16/CH_2	49.5	49.5	0.0	44.5
17/CH	32.5	32.5	0.0	26.7
18/CH_3	21.2	21.2	0.0	22.1
19/CH_3	25.7	25.7	0.0	

[a] Chemical shifts are given in ppm relative to the value obtained for the corresponding calculation on TMS (178.3). [b] Predicted shift = [(experimental shift for that type of carbon in CR iPP) + (difference of calculated shifts)]. Experimental shifts for identifiable defect resonances are given in parentheses. [c] Partially obscured. [d] Is now a proton.

The differences between the calculated values for the copolymer and the homopolymer, which will likely reflect some cancellation of errors, give good agreement with the observed resonances when these differences are applied to the corresponding shift positions of the main CR iPP peaks. The calculated chemical shifts of methylene carbons 4 and 13 are almost unaffected by the transformation from homopolymer to copolymer (difference: −1.4 and 0, respectively). These methylenes should then be hidden beneath the backbone methylene resonance. Significant shifts, relative to the homopolymer, are found for four carbons of the copolymer including the sequence of three methylene carbons (7, 8, and 10) along with methine carbon, no. 5. We observe only three of these four carbons since carbon no. 8, the "central" methylene carbon, is predicted to resonate at 26.7−4.2 or 22.5 ppm where it would be obscured by the main methyl resonance. Note that carbon no. 8 is the only carbon which changes its identity (from CH to CH_2) when converting from homopolymer to copolymer; hence, computational errors may not cancel so well via the "difference" method for this site.

We digress briefly to indicate how we experimentally measured the shift of C8 even though its resonance was

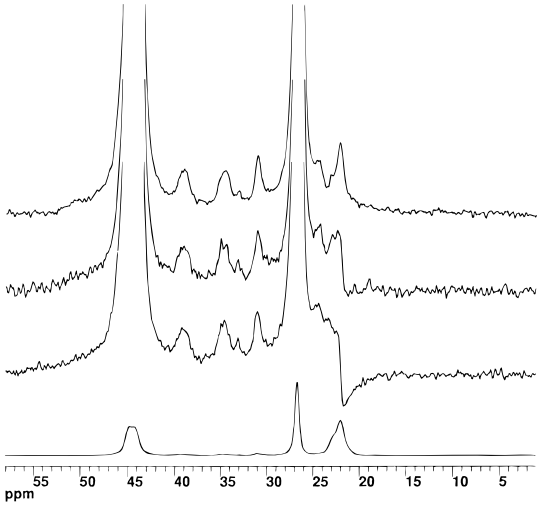

Figure 6. Three polarization/depolarization spectra of the iPP/7.5 Eth sample that were used to establish the chemical shift (24.5 ppm) of the fourth defect-related resonance; this is a CH_2 resonance sandwiched between the main CH and CH_3 resonances. In this experiment, the CP times are split; the first interval is 700 μs followed immediately by a second variable time at the start of which the ^{13}C rf phase is shifted by 180°. In the spectra, from the top down, this second interval is 99, 98, and 97 μs, and these times are chosen to be close to the null condition for the CH_3 resonances. What appears as positive signals in these spectra are those signals (CH and CH_2 carbons) which have already passed through the null condition. The lower spectrum is the scaled-down CR spectrum and is intended simply as a visual reference for the positions of each main resonance. The weak shoulder associated with the 24.5 ppm ethylene-defect resonance remains quite independent of the changes occurring in the CH_3 spectral region. Its visibility is greatly aided by its location between the CH and CH_2 resonances.

mostly obscured. The idea that we used was that the cross-polarization rates for rotating CH_3 carbons are different from relatively rigid CH_2 carbons. We used the "polarization/depolarization" (P/D) method[41] in which we cross-polarized the carbons for the usual 0.7 ms and then did an abrupt 180° phase shift on the carbon rf. This phase shift causes the carbons to move toward a polarization of about the same magnitude but opposite sign. One can choose the length of time for this second cross-polarization step such that one tries to cancel the CH_3 signal. Since the CH_2 carbons are fastest in cross-polarization response (CH carbons are intermediate), the methylene signal will already be quite negative in amplitude when the CH_3 signal is nulled. In this way, one can try to reveal methylene signals hidden beneath methyl signals. P/D spectra, near the CH_3 null, for three closely spaced depolarization times (97, 98, and 99 μs) are shown in Figure 6 along with a strongly attenuated CR spectrum of the iPP/7.5 Eth sample. There is no attempt in the P/D experiment to isolate the spectrum of the CR regions; however, the wide wings associated with the NC regions are strongly attenuated in these P/D spectra. At the same time, there is some nonuniformity of passage of this methyl signal through this null. It is very fortuitous that the C8 signal occurs at 24.5 ppm, just on the edge of both the main methyl and methine resonances (reference the attenuated CR spectrum). One can see that this weak resonance still exhibits a peak; moreover, its peak height is changing much more slowly than the line shape of the methyl region. Also its amplitude, while difficult to judge precisely, could easily be comparable to the other methylene resonances. Hence, we are confident that this is the C8 resonance. Considering the complex change of the methyl line shape in these spectra, it is doubtful whether one could have used the P/D approach to identify the C8 peak if it strongly overlapped the methyl peak. Incidentally, among the three principal defect lines, the weaker relative intensity at 31 ppm in Figure 6 in comparison to Figure 3 helps to verify the assignment of these three defect lines in terms of methylene or methine carbons. Each methylene carbon is expected to contribute more strongly than each methine carbon in these P/D spectra, as is observed.

The calculated chemical shift differences listed in Table 2 indicate that the C5 methine carbon is shifted to lower fields by 4.4 ppm. This agrees very well with the experimental observation. A sharp resonance with narrow line width, similar in nature to the backbone methine resonance, is observed at 31.2 ppm (shifted 4.5 ppm from the main methine resonance). Calculations for methylene carbons, C7 and C10, indicate shifts upfield with respect to the homopolymer of 4.8 and 9.2 ppm, respectively. These also agree very well with the experimental shift differences between the main CH_2 line and the defect methylene carbons, namely, 5.3 ppm (the 39.2 ppm line) and 9.8 ppm (the 34.7 ppm line). Thus, for these three defect carbons, the prediction of chemical shifts based on the difference method gives excellent agreement with experiment (within 0.6 ppm). The central C8 methylene shift is less well predicted by the difference method, i.e., the 4.2 ppm upfield shift, when taken with respect to the 26.7 ppm methine carbon, predicts a shift of 22.5 ppm instead of the 24.5 ppm experimental value. This is a 2.0 ppm difference. However, as mentioned before, the cancellation of computational errors may be thwarted somewhat for C8 by its change of identity in converting from a methine to a methylene carbon. So we regard this computed C8 result as reasonable agreement. Thus, the computations bear out the same assignment as was argued on the basis of γ-gauche and vicinal−gauche interactions and their resulting conformationally induced inequivalences. (We note that the 4.5 ppm shift difference between C7 and C10 is somewhat larger than expected for a difference of one vicinal−gauche interaction. However, we have recently done shift calculations on butane and 2,3-dimethylbutane. For both of these molecules, the vicinal−gauche effect is closer to 4.5 ppm. The details of these computations will be included in a forthcoming publication.)

It is also without doubt that each visible defect resonance represents one carbon per defect. The chemical equivalences of the solution state do *not* carry over into the solid state. The QM calculations are essential to the unambiguous assignment of these resonances and to the establishment of the proper partitioning coefficient. Also, the good agreement between calculated and experimental shifts supports the assumption that the 3_1 helical conformation of the backbone is preserved in the vicinity of the ethylene defect.

Concentration of Ethylene in the Crystal. The resolved character of three of the four ethylene-defect resonances allows us to integrate these lines in the CR spectrum and compare these integrals against the integrals of the main peaks. In so doing, one can deduce the concentration of ethylene repeat units in the CR regions. There are smaller, interfering, intensity contributions arising from stereo and regio defects, in the

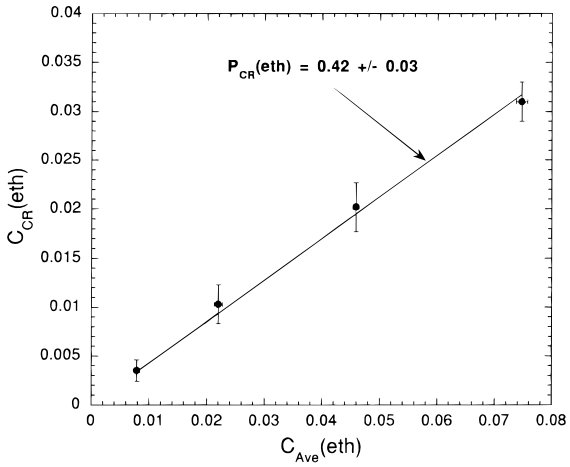

Figure 7. Plot of the mole fraction, in percent, of ethylene in the CR regions against the sample-average mole fraction of ethylene. Error bars represent standard uncertainties.

spectral region between the main CH_2 and CH peaks. However, these resonances are confined to the shift range below 36 ppm;[17] hence, the best ethylene defect resonance for integration is at 39.2 ppm since it is free of contributions from the stereo and regio defects and it is also free of significant overlap with the main resonances. Integration is not straightforward because the line shapes are not expected to be smooth mathematical functions (e.g., Gaussian or Lorentzian) and because each defect resonance is superposed on a slightly curving baseline. Integration of the 39.2 ppm peak was carried out by three different methods. In one integration method, employing a dual spectral display of the identical CR spectrum, the methylene backbone resonance in one spectrum was scaled down and shifted underneath the 39.2 ppm resonance of the other spectrum. Then the scaling factor was adjusted so that, by difference, the intensity in the 39.2 ppm region was approximately nulled. The relative intensity was then extracted from the scaling factor. A second method involved electronic integration following a baseline correction. The third method was cut and weigh. All methods gave similar results.

The ethylene concentration in the crystalline region, C_{CR}(eth), is found to increase from a mole fraction of 0.35% for the iPP/0.8 Eth sample to 3.1% for the iPP/7.5 Eth sample. In Figure 7 the four C_{CR}(eth) values are plotted against the overall ethylene concentration. Figure 7 illustrates that the ethylene uptake in the crystal is, within experimental error, proportional to the overall ethylene content of the chains. According to Figure 7, the P_{CR}(Eth) value is 0.42 ± 0.03 where the given standard uncertainty assumes this latter linear relationship. This P_{CR}(Eth) value indicates that ethylene units can certainly be found in the CR regions; however, there is also significant discrimination against the incorporation of ethylene units into the crystalline region. It follows that, as crystallization proceeds, the concentration of ethylene units in the melt increases; hence, one expects that kinetic as well as thermodynamic factors should be important in dictating the uptake of these defects into the CR regions. On the basis of the observed overall increase in uptake with overall defect concentration, one, by analogy, expects a continuous increase of C_{CR}(eth) and P_{CR}(Eth) during the crystallization of each of these copolymers at a fixed undercooling. Data for the ethylene concentrations and the partitioning coefficients for each sample are listed in Table 3. The above considerations indicate that the C_{CR}(eth) and P_{CR}(Eth) data cited must represent average values incurred during crystallization while slowly cooling from the melt at 1 °C/min.

The constancy of the partitioning coefficient in the copolymer series with increasing ethylene content can be compared with similar data obtained in other types of random copolymers.[42,43] For example, ethylene/vinyl alcohol random copolymers show no discrimination in the partitioning of the hydroxyl groups in the CR or NC regions;[42] hence, the partitioning coefficient is constant with increasing vinyl alcohol content. However, in a series of poly(*β*-hydroxybutyrate-*co*-*β*-hydroxyvalerate) copolymers, the P_{CR}(HV) for the hydroxyvalerate (HV) units increased from 0.36 to 0.74 for overall HV comonomer mole fractions ranging from 4.4 to 27%.[43] This range of defect concentrations is much wider than that explored for the iPP/ethylene copolymers, so a detailed comparison is not feasible. Nevertheless, for the HB−HV copolymer, as the relative number of HV units in the crystal increases, there is a tendency to include a larger fraction of the available HV residues. The suggested rationalization[43] for that trend was that the energy cost of introducing another defect into a CR lattice decreases as the number of defects already in the lattice increases. The partitioning coefficient of the methyl branch of an ethylene propylene copolymer with an overall concentration of 5.6 methyl branches per 1000 carbon atoms was found to be of 0.28 ± 0.04.[44] Thus, the P_{CR}(Prop) in the planar zigzag polyethylene lattice is significantly smaller than the P_{CR}(Eth) in the isotactic polypropylene lattice.

Inspection of the CR line shape of the copolymers studied here allows us to, at least, give qualitative arguments as to the conformation and distribution of the comonomer within the crystalline region, i.e., if the comonomer units are randomly distributed or if a high concentration of these units may pile up on the CR side of the CR/NC interphase. The pertinent experimental observation, as noted earlier, is that the NC spectra (see Figure 1) lack any sharp defect resonances at the

Table 3. Data Related to Ethylene Concentrations, Partitioning Coefficients, Degrees of Crystallinity, Heats of Fusion, and Fractions of All Crystallites in the *γ*-Form for Propylene−Ethylene Copolymers[a]

C_{Ave}(eth)[b] (mole fraction) (%)	C_{CR}(eth)[c] (mol %)	P_{CR}(eth)	crystallinity NMR[d] (±0.03)	P_{NC}(eth)[e]	fraction of total ethylenes in crystal	heat of fusion (J/g) (±6)	*γ*-form (% of CR frac) (±5)
0.79(5)	0.35(11)	0.44(17)	0.66	2.0(3)	0.29(12)	92	45
2.20(7)	1.03(20)	0.47(10)	0.65	2.0(3)	0.30(7)	84	40
4.59(5)	2.02(25)	0.44(6)	0.63	2.0(2)	0.28(5)	68	70
7.47(10)	3.10(20)	0.42(3)	0.58	1.8(2)	0.24(3)	61	100

[a] Standard uncertainties are either given in the column heading or are indicated in parentheses (in units of the least significant digit). [b] Moles of ethylene in 100 total moles of monomer units. [c] Based on integration of the 39 ppm resonance. Moles of ethylene in 100 mol of crystalline repeat units. [d] Based on the CR and NC contributions to the 0 ms SL spectrum and corrections for differing CP efficiencies, including $T_{1\rho}^{H}$ effects. [e] Deduced from other data in this table; not based on direct observation of NC defect carbon resonances.

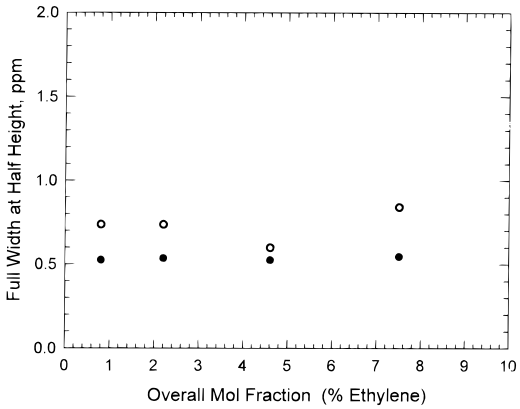

Figure 8. Full width at half-height for two kinds of CH resonance in the CR region: that of the 31.1 ppm ethylene defect (○) and that of the main CH carbon (●); values are plotted against the overall ethylene concentration. Relative constancy and the limited magnitude of the line width ratio suggests that ethylene residues are found in regions of relatively high crystalline order, i.e., not simply crowded at the CR/NC interface (error in fwhh: ±0.05 ppm).

positions seen in the CR spectra. In fact, they lack any distinct defect resonances. On the basis of calculated polarization profiles in a system with an ideally sharp CR/NC interphase, it is predicted[17] that the NC line shape should include a modest positive contribution from the CR side of the interface. (This prediction will not be altered significantly in the presence of an interface of finite width.) Since this is not seen in the NC spectra of these copolymers, we conclude that the ethylene defects are not highly concentrated *on the CR side* of the CR/NC interface. At the same time, we do not regard this observation as disproving the possibility of some gradient of ethylene concentration from the interface to the interior of the CR region. On the other hand, we can reject the notion that all of the ethylene defects in the CR domains lie within 2 nm of the interface.[17] We emphasize again that by this argument we imply *nothing* about the possibility that there is a high concentration of ethylene residues on the NC side of the interface; basically, at ambient temperature, we do not distinguish the NC defect resonances because they are too wide.

A second indication that the ethylene units are most likely dispersed throughout the whole crystalline region is given by the sharpness of the resonances in the CR spectrum associated with the ethylene groups. The line widths (full width at half-height) for the backbone methine resonance at 26.7 ppm and the C5 methine resonance at 31.2 ppm resonance in the crystalline regions are plotted in Figure 8 as a function of the average ethylene content in the chain. The line width for the defect carbon is only slightly broader than that corresponding to the main methine carbon; moreover, these line widths are basically independent of the ethylene content in the range investigated. If a high proportion of ethylene units were found close to the surface of the crystals, in a region with more disorder, a larger difference in line widths would have been expected. The comparable CR line widths for defect-related carbons and for the main iPP carbons of the same type also indicates uniformity in the (3_1 helical) conformation adopted by the ethylene units in the crystal. Also, the constancy of the positions of the main iPP resonances for all samples indicates that the presence of the ethylene units in the CR lattice does not appreciably alter the conformation of the iPP chains.

We also used the NMR data to determine the crystalline mass fractions, i.e., the "NMR crystallinities" (Table 3), and found them to decrease from 0.66 to 0.58 as the ethylene content increased. These crystallinities, in turn, are based on the relative contributions of the CR and NC line shapes to the 0 ms SL spectra including a correction for differences in cross-polarization efficiencies. For our 0.7 ms cross-polarization times, efficiencies were measured to be 3.5 for the CR carbons and 2.8 for the NC carbons. (The latter numbers are ratios of cross-polarized signals to Boltzmann-equilibrium signals, and these numbers automatically correct for differing $T_{1\rho}{}^{H}$ decay rates during cross-polarization.) The decrease in crystallinity values parallels the decrease in the heats of fusion (also listed in Table 3) calculated from the DSC melting endotherms. The larger fractional decrease in the heats of fusion compared with the fractional decrease in crystallinities supports the expected result that the heat of fusion per unit mass of crystalline material is also diminishing as C_{CR}(eth) increases. The trend in both of these latter parameters reflects the *overall inhibition of the crystallization process imposed by the ethylene units despite their partial inclusion in the lattice.*

Using the NMR crystallinities, the fraction of the total ethylenes existing in the CR regions, as opposed to the NC regions, can be computed (Table 3). This fraction is, within experimental error, reasonably constant over the range of overall concentration of ethylene studied. We can also use these crystallinities to deduce the partitioning coefficients, $P_{NC}(\text{eth}) = C_{NC}(\text{eth})/C_{Ave}(\text{eth})$, for the NC region. These values are also quite constant, ranging from 2.0 to 1.8 (Table 3).

Given that there are ethylene defects in the CR lattice, one may ask whether the defects enter the lattice as an equilibrium requirement (forming a solid solution) or as nonequilibrium defects.[45] The linear decrease of the melting temperatures (listed in Table 1) with comonomer composition is consistent with a nonequilibrium defect inclusion. Contrasting with this, it was concluded[46] that the directly bonded methyl groups of ethylene/propylene copolymers of low propylene content enter the polyethylene lattice on an equilibrium basis because a maximum was found in the melting temperature/composition relation for this type of copolymer.

If one simply considers the fact that after the crystallization process is complete in these copolymers, P_{NC}(eth) is about 2, then it is clear that the defect composition of the melt changes during crystallization since, at the very early stages of crystallization, the effective P_{NC}(eth) would be close to 1. Given the observed invariance of P_{CR}(eth) with changes in ethylene concentration, one would anticipate that, as crystallization proceeded and the melt became more concentrated in ethylene defects, the defect concentration in the CR regions would increase for those crystallites formed later in the crystallization process. A constantly changing defect concentration in the melt during, say, isothermal crystallization, would also tend to reduce the effective undercooling as a function of increasing time. All these factors complicate any prediction of the crystalline ethylene concentration in these type of copolymers.

A relevant issue that follows relates to the generality of the measured C_{CR}(eth) values or whether these values are sensitive to thermal history (undercooling). In a

preliminary experiment the iPP/7.5 Eth sample was isothermal crystallized at 115 °C over a 10 day period followed by a slow ramping down of the temperature to ambient temperature over 2 days. About half of the final amount of crystalline material forms at 115 °C, and the other half forms upon cooling. This sample had a C_{CR}(eth) value (spectra and data not shown) indistinguishable from that of the sample cooled at 1 °C/min; hence, in this limited experience, the dependence of C_{CR}(eth) on thermal history seems minimal. It is expected that the C_{CR}(eth) of the crystals formed at 115 °C would be significantly lower than for those formed during our usual cooling at 1 °C/min from the melt because of the more extensive crystallization in the latter case. It is also implied that in the isothermally crystallized sample the crystals formed upon slow cooling from 115 °C to room temperature contain a higher C_{CR}(eth) than those formed at 115 °C. The value of C_{CR}(eth) obtained at room temperature for this sample is, no doubt, an average value of the increasing C_{CR}(eth) during crystallization. Ideally, the test whether C_{CR}(eth) is a function of undercooling could be carried out by analyzing the CPMAS ^{13}C NMR spectra obtained at a given crystallization temperature and never cooled. Of interest are crystallizations that encompass most of the isothermal transformation at relatively low undercoolings (yielding small overall crystallinities). Such crystallizations should minimize the effects on the C_{CR}(eth) from the changing concentration of ethylene in the melt. However, these experiments would be very difficult because of the very long times of signal averaging and the need for long-term temperature stability during crystallization.

Both significant[47] and insignificant[17,43] variations of the concentration of defects in the crystal with thermal history have been found in other systems. If the value of C_{CR}(eth) is subject to thermal history, then one would expect that parameters such as the heat of fusion per mole of crystalline units would be a function of the crystallization temperature. This value is needed, for example, to determine the degree of crystallinity from heat of fusion. The value of C_{CR}(eth) is also of relevance in the calculation of the equilibrium melting temperatures T_m^o of these types of copolymers.[48] In a forthcoming publication we will address experimentally the thermal and kinetics factors affecting the value of C_{CR}(eth) for a fixed overall ethylene content. We will also offer partitioning results for other types of random propylene copolymers.

Conclusions

A series of metallocene-catalyzed propylene/ethylene random copolymers with ethylene contents ranging from mole fractions of 0.8−7.5% and melt crystallization histories of cooling at 1 °C/min were investigated. The partitioning coefficient, P_{CR}(eth), for ethylene residues in the crystalline (CR) regions of these iPP/Eth copolymers has been determined (P_{CR}(eth) = 0.42 ± 0.03) using solid-state ^{13}C NMR methods, including the separation of signals from the CR and the noncrystalline (NC) regions. This partitioning coefficient is defined as the ratio of ethylene concentration in the CR regions to the sample-average concentration of ethylene. P_{CR}(eth) is constant for all samples, including one with a much slower cooling history.

Essential for the determination of P_{CR}(eth) is the proper assignment of the four observed new resonances associated with the ethylene repeat unit. This assignment was made on the basis of quantum mechanical chemical shift calculations for two types of oligomeric chains, 6.5 monomers in length. One chain represented the defect-free iPP chain and the other a chain containing a central ethylene repeat unit. Backbone carbons were confined to a 3_1 helical conformation in both chains; this is the conformation of the individual chains in the CR lattice. The computed shifts were not accurate enough to make assignments. However, we reasoned that if the calculations made systematic approximations unique to the carbon type (e.g., methylene, methyl, etc.), then one could take the computed shift differences, for corresponding carbons on the two types of chains, and go on to predict resonance positions as displacements from the experimental shifts of the defect-free, crystalline iPP chain. That approach worked well, and agreement between calculated and experimental shifts for the defect resonances was good. We could also rationalize the defect-resonance positions reasonably well on the basis of the geometry of the 3_1 helix and the changes in γ-gauche and vicinal−gauche interactions for such a helical structure when an ethylene repeat unit replaces the propylene repeat unit.

On the basis of estimates of crystallinity from the NMR data, we used the P_{CR}(eth) values to deduce the fraction of the total ethylene residues that are found in the CR regions (about 0.27) and the ratio of ethylene concentration in the NC regions to the sample-average concentration (1.9 ± 0.2).

Since spin diffusion modeling indicates that the line shapes of the CR and the NC regions are somewhat distorted, we took advantage of this distortion to investigate the hypothesis that the ethylene defects are highly concentrated at the CR/NC interface. We concluded that they are not highly concentrated there although we cannot prove that they are *uniformly* distributed throughout the CR regions.

It is a challenge to describe the details of crystallization when defects, like this ethylene defect, are taken into the crystalline regions but with some degree of rejection. We intend to investigate some of these issues experimentally.

Acknowledgment. The authors thank Dr. J. C. Randall of Exxon for stimulating and valuable discussions as well as assistance in the analysis of the high-resolution NMR data. Technical assistance of T. E. Gedris of FSU with the solution NMR spectra and of R. Fu of the National High Field Magnetic Laboratory in Tallahassee is also acknowledged. R.G.A. acknowledges support of this work by the National Science Foundation, Polymer Program (DMR-9753258).

Appendix

At the strong recommendation of one referee during the review process for this paper, we also prepared a 0.2 mm thick film of sample iPP/2.2 Eth. This sample was air-cooled relatively rapidly from the melt as a film sandwiched between layers of aluminum foil. The partitioning ratio, P_{CR}(eth), did not differ from the 0.42 obtained when the sample was cooled at 1 °C/min. Moreover, the NMR-based degree of crystallinity of the air-cooled sample (64%) is only slightly lower than the value for the one cooled at 1 °C/min (66%). In contrast, the difference in heat of fusion, 65 and 85 J/g, respectively, between these samples was substantial. The NMR method measures the fraction of residues occupy-

ing ordered 3/1 helical (crystalline) sites. The DSC heat of fusion, on the other hand, averages energy characterizing those crystalline regions. In iPP it is likely that the degree of perfection in the packing of these CR helices (involving C_{CR}(eth), fold surfaces, different allomorphs, pairings of helical handedness, and ordering of "up" and "down" directions for the chains) offers a nontrivial contribution to the heat of melting and that some or all of these parameters are influenced by the rate of cooling. In support of that point of view, we also note that the NMR "CR" line shapes for the two samples showed significant differences in the methyl and methylene regions which likely reflect changes in degree of helical ordering.[34] The data cited in this paragraph certainly complicate the interpretation of heats of fusion in terms of the role that defects play in determining such heats.

References and Notes

(1) Arnold, M.; Henscheke, O.; Knorr, J. *Macromol. Chem. Phys.* **1996**, *197*, 563.
(2) Perez, E.; Benavente, R.; Bello, A.; Pereña, J. M.; Zucchi, D.; Sacchi, M. C. *Polymer* **1997**, *38*, 5411.
(3) Zimmermann, H. J. *J. Macromol. Sci., Phys.* **1993**, *B(32)2*, 141.
(4) Laihomen, S.; Gedde, U. W.; Werner, P. E.; Westdahl, M.; Jääskeläinen, Martinez-Salazar, J. *Polymer* **1997**, *38*, 371.
(5) Busico, U.; Corradini, P.; De Rosa, C.; di Benedetto, E. *Eur. Polym. J.* **1985**, *21*, 239.
(6) Laihonen, S.; Gedde, U. W.; Werner, P.-E.; Martinez-Salazar, J. *Polymer* **1997**, *38*, 361.
(7) Monasse, B.; Haudin, J. M. *Colloid Polym. Sci.* **1988**, *266*, 679.
(8) Turner-Jones, A. *Polymer* **1971**, *12*, 487.
(9) Feng, Y.; Jin, X.; Hay, J. N. *J. Appl. Polym. Sci.* **1998**, *68*, 381.
(10) Avella, M.; Martuscelli, E.; Della Volpe, G.; Segre, A.; Rossi, E. *Macromol. Chem.* **1986**, *187*, 1927.
(11) Crispino, L.; Martuscelli, E.; Pracella, M. *Makromol. Chem.* **1980**, *181*, 1747.
(12) Alamo, R. G.; Mandelkern, L. *Thermochim. Acta* **1994**, *238*, 155 and references therein.
(13) Chi, C. Thesis Dissertation, Florida State University, 1997.
(14) Starkweather, H. W., Jr.; Van-Catledge, F. A.; MacDonald, R. N. *Macromolecules* **1982**, *15*, 1600.
(15) Feng, Y.; Hay, J. N. *Polymer* **1998**, *39*, 6589.
(16) Randall, J. C. *Macromolecules* **1997**, *30*, *803*.
(17) VanderHart, D. L.; Alamo, R. G.; Nyden, M. R.; Kim, M. H.; Mandelkern, L. *Macromolecules* **2000**, *33*, 6078.
(18) Cheeseman, J. R.; Trucks, G. W.; Keith, T.; Frish, M. *J. Chem. Phys.* **1996**, *104*, 5497.
(19) Brintzinger, H. H.; Fischer, D.; Mülhaup, R.; Rieger, B.; Waymouth, R. M. *Angew. Chem., Int. Ed. Engl.* **1995**, *34*, 1143.
(20) Westerman, L.; Clark, J. C. *J. Polym. Sci., Polym. Phys. Ed.* **1973**, *11*, 559.
(21) Randall, J. C. *Macromolecules* **1978**, *11*, 33. Tritto, I.; Fan, Z.-Q.; Locatelli, P.; Sacchi, M. C.; Camurati, I.; Galimberti, M. *Macromolecules* **1995**, *28*, 3342. Busico, V.; Cipullo, R.; Corradini, P.; De Biasio, R. *Macromol. Chem. Phys.* **1995**, *196*, 491. Kakugo, M.; Naito, Y.; Mizunama, K.; Miyatake, T. *Macromolecules* **1982**, *15*, 1150. Zambelli, A.; Sacchi, M. C.; Locatelli, P. *Macromolecules* **1979**, *12*, 783.
(22) Certain commercial companies are named in order to specify adequately the experimental procedure. This in no way implies an endorsement or recommendation by the authors or their agencies.
(23) VanderHart, D. L.; Perez, E. *Marcromolecules* **1986**, *19*, 1902.
(24) *The Principles of Nuclear Magnetism*; Abragam, A., Ed.; Oxford University Press: New York, 1961; Chapter V.
(25) VanderHart, D. L.; Earl, W. L.; Garroway, A. N. *J. Magn. Reson.* **1981**, *44*, 361.
(26) Alamo, R. G.; Kim, M.-H.; Galante, M. J.; Isasi, J. R.; Mandelkern, L. *Macromolecules* **1999**, *32*, 4050.
(27) Brückner, S.; Meille, S. V. *Nature* **1989**, *340*, 455.
(28) Meille, S. V.; Brückner, S.; Porzio, W. *Macromolecules* **1990**, *23*, 4114.
(29) Natta, G.; Corradini, P. *Suppl. Nuovo Cimento* **1960**, *15*, 40.
(30) Mencik, Z. *J. Makromol. Sci., Phys.* **1972**, *B6*, 101.
(31) Hikosaka, M.; Seto, T. *Polym. J.* **1973**, *5*, 111.
(32) Brückner, S.; Meille, S. V.; Sozzani, P.; Torri, G. *Makromol. Chem. Rapid Commun.* **1990**, *11*, 55.
(33) Gomez, M. A.; Tanaka, H.; Tonelli, A. E. *Polymer* **1987**, *28*, 2227.
(34) Caldas, V.; Brown, G. R.; Nohr, R. S.; MacDonald, J. G. *J. Polym. Sci., Part B: Polym. Phys. Ed.* **1996**, *34*, 2085.
(35) Tonelli, A. E. *Macromolecules* **1978**, *11*, 565, 634.
(36) Möller, M.; Gronski, W.; Cantow, H.-J.; Höcker, H. J. *J. Am. Chem. Soc.* **1984**, *106*, 5093.
(37) Natta, G.; Corradini, P. *Suppl. Nuovo Cimento* **1960**, *15*, 40.
(38) Gaussian 98 (Revision A.2): Frisch, M. J.; Trucks, G. W.; Schlegel, H. B.; Scuseria, G. E.; Robb, M. A.; Cheeseman, J. R.; Zakrzewski, V. G.; Montgomery, J. A.; Stratmann, R. E.; Burant, J. C.; Dapprich, S.; Millam, J. M.; Daniels, A. D.; Kudin, K. N.; Strain, M. C.; Farkas, O.; Tomasi, J.; Barone, V.; Cossi, M.; Cammi, R.; Mennucci, B.; Pomelli, C.; Adamo, C.; Clifford, S.; Ochterski, J.; Petersson, G. A.; Ayala, P. Y.; Cui, Q.; Morokuma, K.; Malick, D. K.; Rabuck, A. D.; Raghavachari, K.; Foresman, J. B.; Cioslowski, J.; Ortiz, J. V.; Stefanov, B. B.; Liu, G.; Liashenko, A.; Piskorz, P.; Komaromi, I.; Gomperts, R.; Martin, R. L.; Fox, D. J.; Keith, T.; Al-Laham, M. A.; Peng, C. Y.; Nanayakkara, A.; Gonzalez, C.; Challacombe, M.; Gill, P. M. W.; Johnson, B. G.; Chen, W.; Wong, M. W.; Andres, J. L.; Head-Gordon, M.; Replogle, E. S.; Pople, J. A. Gaussian, Inc., Pittsburgh, PA, 1998.
(39) Becke, A. D. *J. Chem. Phys.* **1993**, *98*, 5648.
(40) Lee, C.; Yang, W.; Parr, R. G. *Phys. Rev. B* **1988**, *37*, 785.
(41) Wu, X. L.; Zilm, K. W. *J. Magn. Reson., Ser. A* **1993**, *102*, 205.
(42) VanderHart, D. L.; Simmons, S.; Gilman, J. W. *Polymer* **1995**, *36*, 4223.
(43) VanderHart, D. L.; Orts, W. J.; Marchessault, R. H. *Macromolecules* **1995**, *28*, 6394.
(44) Perez, E.; VanderHart, D. L. *J. Polym. Sci., Part B: Polym. Phys. Ed.* **1987**, *25*, 1637.
(45) Richardson, M. J.; Flory, P. J.; Jackson, J. B. *Polymer* **1963**, *4*, 221.
(46) Baker, C. H.; Mandelkern, L. *Polymer* **1966**, *7*, 71.
(47) Yoshie, N.; Sakurai, M.; Inoue, Y.; Chûjô, R. *Macromolecules* **1992**, *25*, 2048.
(48) Sanchez, I. C.; Eby, R. K. *Macromolecules* **1975**, *8*, 638.

MA000267I